Article

# Supramolecular Assembly of Dendritic Polymers Elucidated by H and C Solid-State MAS NMR Spectroscopy

Almut Rapp, Ingo Schnell, Daniel Sebastiani, Steven P. Brown, Virgil Percec, and Hans Wolfgang Spiess

*J. Am. Chem. Soc.*, **2003**, 125 (43), 13284-13297• DOI: 10.1021/ja035127d • Publication Date (Web): 03 October 2003



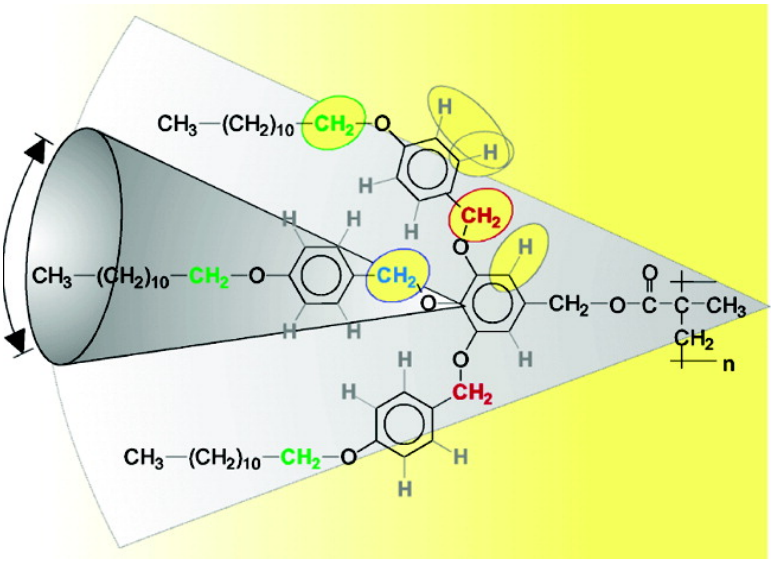

## More About This Article

Additional resources and features associated with this article are available within the HTML version:

- Supporting Information
- Links to the 9 articles that cite this article, as of the time of this article download
- Access to high resolution figures
- Links to articles and content related to this article
- Copyright permission to reproduce figures and/or text from this article

View the Full Text HTML

J|A|C|S
ARTICLES
Published on Web 10/03/2003

# Supramolecular Assembly of Dendritic Polymers Elucidated by $^{1}H$ and $^{13}C$ Solid-State MAS NMR Spectroscopy

Almut Rapp,[†] Ingo Schnell,[†] Daniel Sebastiani,[†] Steven P. Brown,[†,‡] Virgil Percec,[§] and Hans Wolfgang Spiess*,[†]

*Max Planck Institute for Polymer Research, Postfach 3148, 55021 Mainz, Germany and Roy and Diana Vagelos Laboratories, Department of Chemistry, University of Pennsylvania, Philadelphia, Pennsylvania 19104-6323*

Received March 13, 2003; E-mail: spiess@mpip-mainz.mpg.de

***Abstract:*** Advanced solid-state NMR methods under fast magic-angle spinning (MAS) are used to study the structure and dynamics of large supramolecular systems, which consist of a polymer backbone with dendritic side groups and self-assemble into a columnar structure. The NMR experiments are performed on as-synthesized samples, i.e., no isotopic enrichment is required. The analysis of $^{1}H$ NMR chemical-shift effects as well as dipolar $^{1}H-^{1}H$ or $^{1}H-^{13}C$ couplings provide site-specific insight into the local structure and the segmental dynamics, in particular, of phenyl rings and $-CH_2O-$ linking units within the dendrons. Relative changes of $^{1}H$ chemical shifts (of up to $-3$ ppm) serve as distance constraints and allow protons to be positioned relative to aromatic rings. Together with dipolar spinning sideband patterns, $\pi-\pi$ packing phenomena and local order parameters (showing variations between 30% and 100%) are selectively and precisely determined, enabling the identification of the dendron cores as the structure-directing moieties within the supramolecular architecture. The study is carried out over a representative selection of systems which reflect characteristic differences, such as different polymer backbones, sizes of dendritic side groups, or length and flexibility of linking units. While the polymer backbone is found to have virtually no effect on the overall structure and properties, the systems are sensitively affected by changing the generation or the linkage of the dendrons. The results help to understand the self-assembly process of dendritic moieties and aid the chemical design of self-organizing molecular structures.

## 1. Introduction

Determining the structure as well as identifying the structure-driving and structure-directing features of supramolecular systems represent an important challenge for modern characterization techniques in the rapidly developing field of supramolecular chemistry.[1]In this paper we demonstrate how advanced solid-state NMR methods under fast magic-angle spinning (MAS) can provide detailed information about the structure and dynamics of fairly large supramolecular systems without isotopic enrichment. In this context, solid-state NMR has recently made considerable progress in the field of complex biomolecular systems.[2] In the work presented here, MAS frequencies of 30 kHz combined with dipolar $^{1}H-^{1}H$ or $^{1}H-^{13}C$ recoupling techniques[3] give insight into the local structure of several related self-assembling columnar structures.[4] These superstructures are formed by polymer molecules consisting of a polymethacrylate (PMA) or polystyrene (PS) backbone with large dendritic side groups.[5] In particular, site-specific information about the local dynamics of different $CH_n$ units is obtained, which allows the identification of the structure-driving and structure-determining elements in the self-assembly process of such systems. The following four related polymers were investigated:[6]

[†] Max Planck Institute for Polymer Research.
[‡] Present address: Department of Physics, University of Warwick, Coventry CV4 7AL, U.K.
[§] University of Pennsylvania.

(1) (a) Steed, J. W.; Atwood, J. L. *Supramolecular Chemistry*; Wiley: 2000. (b) Ciferri, A. *Supramolecular Polymers*; Dekker: New York, 2000. (c) Atwood, J. L.; Lehn, J.-M. *Comprehensive Supramolecular Chemistry*; Pergamon Press: Oxford, 1996; Vols. 9 and 10. (d) Ciferri, A. *Macromol. Rapid Comm.* **2002**, *23*, 511−529. (e) Gorp, J. J.; Vekemans, J. A. J. M.; Meijer, E. W. *J. Am. Chem. Soc.* **2002**, *124*, 14759−14769. (f) Ma, Y.; Kolotuchin, S. V.; Zimmerman, S. C. *J. Am. Chem. Soc.* **2002**, *124*, 13757−13769. (g) Fenniri, H.; Deng, B.-L.; Ribbe, A. E. *J. Am. Chem. Soc.* **2002**, *124*, 11064−11072. (h) Brunsveld, L.; Folmer, B. J. B.; Meijer, E. W.; Sijbesma, R. P. *Chem. Rev.* **2001**, *101*, 4071−4097. (i) Moore, J. S. *Curr. Opin. Colloid In.* **1999**, *4*, 108−116. (j) Suárez, M.; Lehn, J.-M.; Zimmerman, S. P.; Skoulios, A.; Heinrich, B. *J. Am. Chem. Soc.* **1998,** *120*, 9526−9532.

(2) (a) Creemers, A. F. L.; Kiihne, S.; Bovee-Geurts, P. H. M.; DeGrip, W. J.; Lugtenburg, J.; de Groot, H. J. M. *Proc. Natl. Acad. Sci. U.S.A.* **2002**, *99*, 9101−9106. (b) Luca, S.; Filippov, D. V.; van Boom, J. H.; Oschkinat, H.; de Groot, H. J. M.; Baldus, M. *J. Biomol. NMR* **2001**, *20*, 325−331. (c) Alia; Matysik, J.; Soede-Huijbregts, C.; Baldus, M.; Raap, J.; Lugtenburg, J.; Gast, P.; van Gorkom, H. J.; Hoff, A. J.; de Groot, H. J. M. *J. Am. Chem. Soc.* **2001**, *123*, 4803−4809. (d) van Rossum, B. J.; Steensgaard, D. B.; Mulder, F. M.; Boender, G. J.; Schaffner, K.; Holzwarth, A. R.; de Groot, H. J. M. *Biochemistry* **2001**, *40*, 1587−1595. (e) Rienstra, C. M.; Hohwy, M.; Mueller, L. J.; Jaroniec, C. P.; Reif, B.; Griffin, R. G. *J. Am. Chem. Soc.* **2002**, *124*, 11908−11922. (f) Rienstra, C. M.; Tucker-Kellogg, L.; Jaroniec C. P.; Hohwy, M.; Reif, B.; McMahon, M. T.; Tidor, B.; Lozano-Perez, T.; Griffin, R. G. *Proc. Natl Acad. Sci. U.S.A.* **2002**, *99*, 10260−10265. (g) van Beek, J. D.; Hess, S.; Vollrath, F.; Meier, B. H. *Proc. Natl. Acad. Sci. U.S.A.* **2002**, *99*, 10266−10271.

(3) Brown, S. P.; Spiess, H. W. *Chem. Rev.* **2001**, *101*, 4125−4155.

(4) Percec, V.; Ahn, C.-H.; Ungar, G.; Yeardley, D. J. P.; Möller, M.; Sheiko, S. S. *Nature* **1998**, *391*, 161−164.

(5) Dendritic polymers in general: (a) Newkome, G. R.; Moorefield, C. N.; Vögtle, F. *Dendritic Macromolecules;* VCH: Weinheim, 1996 (b) Vögtle, F. *Top. Curr. Chem.* **1998**, *197*, 19−77 and 165−191; Vögtle, F. *Top. Curr. Chem.* **2001**, *212*, 41−80. Vögtle, F. *Top. Curr. Chem.* **2001**, *217*, 1−50 and 95−120. (c) Frey, H. *Angew. Chem., Int. Ed.* **1998**, *37*, 2193−2197.


**10.1021/ja035127d CCC: $25.00** 

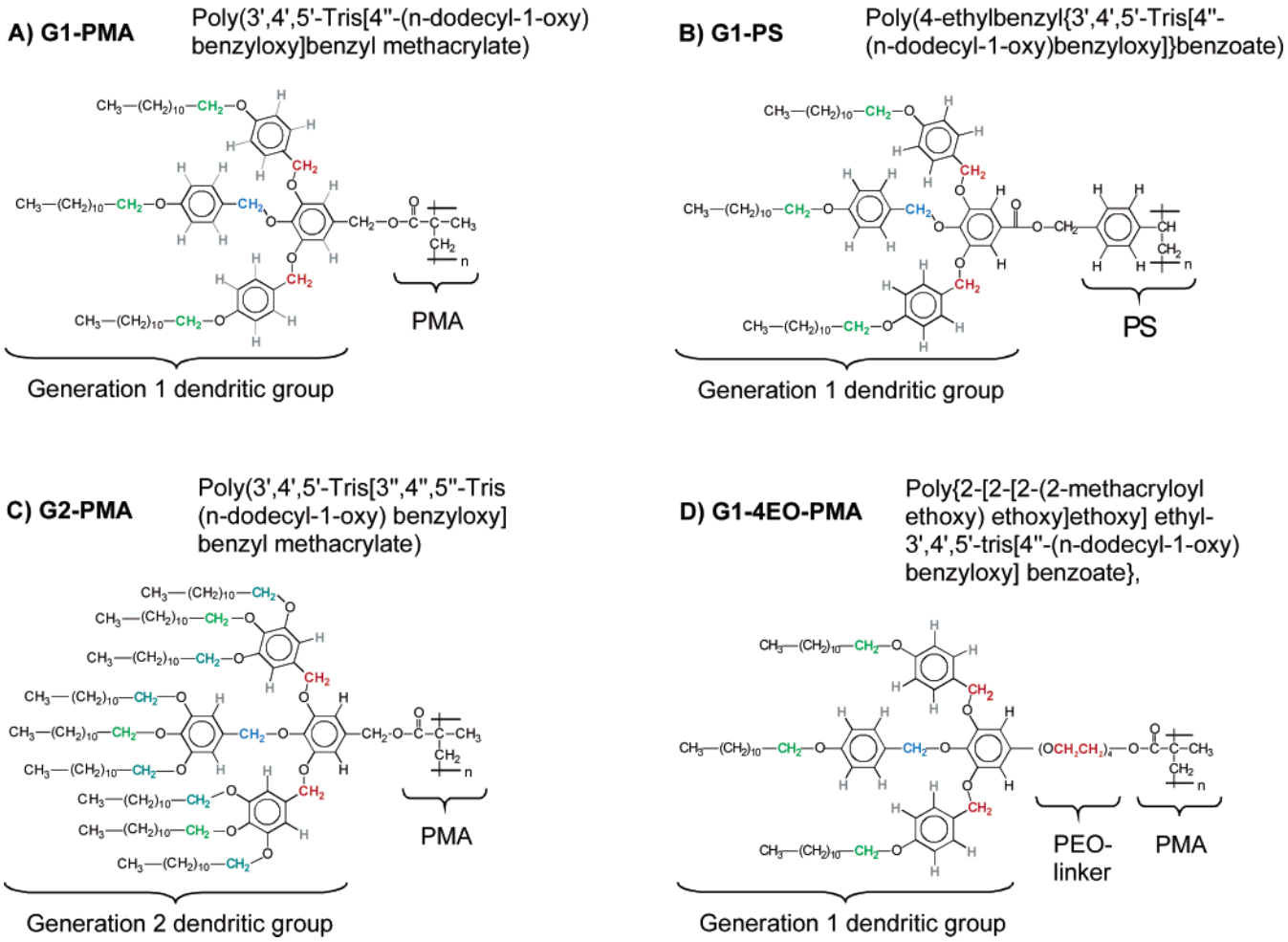


***Figure 1.*** Systems investigated in this study. All consist of a polymer backbone (PMA or PS) to which dendrons of first and second generation (G1 and G2) are attached. The side groups are responsible for a columnar supramolecular arrangement of the molecules.

(A) poly(3′,4′,5′-tris[4′′-(*n*-dodecyl-1-oxy)benzyloxy]benzylmethacrylate), henceforth referred to as **G1-PMA**,

(B) poly(4-ethylbenzyl{3′,4′,5′-tris[4′′-(*n*-dodecyl-1-oxy)-benzyloxy]}benzoate), henceforth referred to as **G1-PS**,

(C) poly(3′,4′,5′-tris[3′′,4′′,5′′-tris(*n*-dodecyl-1-oxy)benzyloxy]benzylmethacrylate), henceforth referred to as **G2-PMA**, and

(D) poly{2-[2-[2-(2-methacryloylethoxy)ethoxy]ethoxy]ethyl-3′,4′,5′-tris[4′′-(*n*-dodecyl-1-oxy)benzyloxy]benzoate}, henceforth referred to as **G1-4EO-PMA**.

The dendrons are attached to a polymer backbone by a short and inflexible $-CH_2OCO-/-COOCH_2Ph-$ linking unit or by a more extended and flexible $-(OCH_2CH_2)_4OCO-$ unit (see Figure 1). They self-organize in a columnar fashion in the solid state, as shown by scanning force microscopy.[6a] G1-4EO-PMA has also been studied in great detail by small and wide-angle X-ray diffraction.[7] G1-PMA, G1-PS, and G1-4EO-PMA display a glass transition temperature, while G2-PMA does not. The observed liquid crystalline phase is hexagonal columnar $\phi_h$,[6a] which shows that the highly organized columnar structure is observed below as well as above $T_g$.

The paper is structured as follows: After providing a brief overview of the NMR methods applied, the structural features and segmental dynamics (below $T_g$) of G1-PMA (see Figure 1A) are studied by analyzing $^1H$ NMR chemical shifts as well as $^1H-^{13}C$ and $^1H-^1H$ dipolar sideband patterns. In particular, the aromatic rings and the $-CH_2O-$ linking units within the dendrons are investigated in detail. On the basis of the high degree of local order found within the dendrons, they are identified as the structure-directing moieties of the columnar architecture. Subsequently, the results obtained for G1-PMA are systematically compared to materials with characteristic differences, i.e., a different polymer backbone (G1-PS, see Figure 1B), a larger dendritic side group (G2-PMA, see Figure 1C), and, finally, a longer and more flexible linker between backbone and dendron (G1-4EO-PMA, see Figure 1D).

## 2. NMR Theory and Methods

**2.1. Dipole−Dipole Couplings and Magic-Angle Spinning (MAS).** All solid-state NMR methods applied in this work are based on the effective suppression and/or the measurement of homo- and heteronuclear dipole−dipole couplings which depend on both the distance between the two spins involved as well as

(6) (a) Percec, V.; Ahn, C.-H.; Cho, W.-D.; Jamieson, A. M.; Kim, J.; Leman, T.; Schmidt, M.; Gerle, M.; Möller, M.; Prokhorova, S. A.; Sheiko, S. S.; Cheng, S. Z. D.; Zhang, A.; Ungar, G.; Yeardley, D. J. P. *J. Am. Chem. Soc.* **1998**, *120*, 8619−8631. (b) Percec, V.; Heck, J.; Tomazos, D.; Falkenberg, F.; Blackwell, H.; Ungar, G. *J. Chem. Soc., Perkin Trans.* **1993**, *1*, 2799−2811.

(7) (a) Chvalun, S. N.; Shcherbina, M. A.; Bykova, I. V.; Blackwell, J.; Percec, V.; Kwon Y. K.; Cho, J. D. *Polym. Sci A.* **2001**, *43*, 33−43. (b) Chvalun, S. N.; Blackwell, J.; Cho, J. D.; Bykova, I. V.; Percec, V. *Acta Polym.* **1999**, *50*, 51−56. (c) Kwon Y. K.; Chvalun, S. N.; Blackwell, J.; Percec, V.; Heck, J. *Macromolecules* **1995**, *28*, 1552−1558.

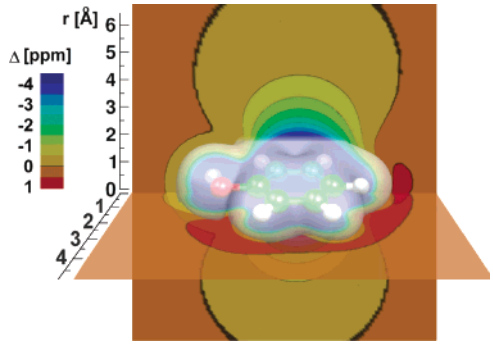


***Figure 2.*** Nucleus-independent chemical-shift (NICS)[8] map of a phenol ring, calculated using density functional theory with the BLYP exchange-correlation functional[9] and the CPMD code.[10] The color code reflects the chemical-shift change a nucleus would experience when placed at the respective position relative to the phenol ring. The white-shaded surface around the phenol molecule represents the effective exclusion volume where no other atom can be placed without strongly interfering with the phenol electrons.

on the molecular dynamics. The distance dependence of the coupling is contained in the dipolar coupling constant $D_{ij} = -(\mu_0\hbar\gamma_i\gamma_j)/(4\pi r_{ij}^3)$, where $r_{ij}$ denotes the internuclear distance and $\gamma_{i,j}$ the magnetogyric ratios of the nuclei. The dependence on the molecular dynamics arises from the anisotropy of the interaction in the presence of a strong magnetic field ($B_0$), which is proportional to $(3\cos^2\theta - 1)$, where $\theta$ is the angle between the internuclear vector and the $B_0$ field. In solid-state NMR, dipole−dipole interactions are known to broaden the resonance lines and hamper spectral resolution of molecular building blocks according to their chemical shifts. In this work, fast MAS at rotation frequencies of 25−30 kHz and high $B_0$ fields (corresponding to a $^1$H Larmor frequency of 700 MHz) are applied to ensure sufficient resolution even in $^1$H spectra.

**2.2. Distance Constraints from $^1$H Chemical-Shift Effects of Aromatic Ring Currents.** $^1$H chemical shifts are known to be affected by aromatic ring currents and be indicative of supramolecular organization.[3] Pronounced effects of such kind are also observed in the dendritic side chains of the systems studied here. Our present work includes model calculations in order to arrive at a more quantitative interpretation and to relate the characteristic $^1$H shift effects to local structural features. For a better understanding of the possible molecular origins of the observed up- and downfield shifts of individual protons, a nucleus-independent chemical-shift (NICS) map[8] of a phenol ring has been computed, as shown in Figure 2. Although the phenol system is quite small, the calculation has been performed using a DFT method, because it is capable of handling also larger and more complex systems, to which we plan to extend our work in the future. The accuracy of this approach is checked as described below.

A NICS map[8] is a generalization of the atom-specific chemical shift tensor. It is defined as the trace of the shielding tensor computed at every point in space, as opposed to the traditional chemical shielding value which is only calculated at the positions of the nuclei. The map shows how much the chemical shift of a fictitious nuclear spin would be changed by the presence of a particular molecule. Technically, we calculate the electronic linear response to the external magnetic field, which results in an electronic current density. This quantum current induces an additional magnetic field within a range of several angstroms, which is the basis of our NICS maps. Taken at the actual positions of the atoms, we would find their absolute chemical shielding values. In this calculation, no explicit probe atom is incorporated, such that the picture is quantitative only in the limit of noninteracting molecules. However, as long as the electronic wave functions do not overlap with those of neighboring molecules, it can be assumed that the electronically induced magnetic fields are essentially unchanged.

The calculations were performed in the framework of density functional theory with the BLYP exchange-correlation functional[9] using the CPMD code.[10] The electronic orbitals were expanded in plane waves with a cutoff of 70 Ry, and Goedecker-type pseudopotentials[11] were used for all atoms. The system was put in a large unit cell of 20 Å$^3$ in order to eliminate interactions between periodic images. The magnetic response properties were calculated using the method described in ref 12.[12] Prior to calculating the NICS map, the geometry of the molecule was fully optimized under the same computational setup.

The resulting map (see Figure 2) displays the theoretical chemical-shift displacement that a nuclear spin would experience when placed at a given position relative to a phenol molecule. Such rings represent key building blocks of the dendrons under investigation. In their environments, characteristic chemical-shift patterns are thus expected with large and long-ranged $\pi$-shifts (to lower frequencies) above and below the ring, as well as a weak and localized inverse effect beside the ring. On the basis of the map in Figure 2, the shift effect experienced by a proton can be used in a semiquantitative fashion to locate the proton relative to the aromatic ring. The shift effects are determined by comparing $^1$H NMR spectra of dilute solutions (with negligible aggregation of the solubilized molecules) with solid-state data. For example, a proton in the condensed phase that is shifted to lower frequency by $\Delta = \delta_{solid} - \delta_{solution} = -2$ ppm can be expected within a distance range of 2−3 Å above or below the center of a phenyl ring. In this way, the $^1$H chemical shift can provide distance constraints for the structure, which are remarkably precise given the simplicity of the approach. In biological solid-state NMR, such $^1$H chemical-shift constraints have already been used successfully in a study of bacteriochlorophyll aggregates.[2d] Moreover, in materials research, solid-state structures have been derived by combining experimental $^1$H shifts with quantum-chemical calculations.[13,14]

To determine the accuracy of the NICS scheme and its implementation in the CPMD code, we performed a comparative all-electron ab initio calculation of a system containing a benzene and methane molecule in various geometries. The methane molecule was placed at about 150 characteristic positions within the "shielding cone" of the benzene molecule, and its proton NMR chemical shifts (relative to the isolated

(8) Ragué Schleyer, P.; Maerker, C.; Dransfeld, A.; Jiao, H.; van Eikema Hommes, N. J. R. *J. Am. Chem. Soc.* **1996**, *118*, 6317−6318.

(9) (a) Becke, A. D. *Phys. Rev. A* **1988**, *38*, 3098−3100. (b) Lee, C. T.; Yang, W. T.; Parr, R. G. *Phys. Rev. B* **1988**, *37*, 785−789.

(10) Computer program CPMD V3.5, http://www.cpmd.org, IBM Corp., 1990−2001, Max-Planck-Institut für Festkörperforschung, Stuttgart 1997−2001.

(11) Goedecker, S.; Teter, M.; Hutter, J. *Phys. Rev. B* **1996**, *54*, 1703−1710.

(12) Sebastiani, D.; Parrinello, M. *J. Phys. Chem. A* **2001**, *105*, 1951−1958.

(13) (a) Ochsenfeld, C.; Koziol, F.; Brown, S. P.; Schaller, T.; Seelbach, U. P.; Klärner, F.-G. *Solid State Nucl. Magn. Reson.* **2002**, *22*, 128−153. (b) Brown, S. P.; Schaller, T.; Seelbach, U. P.; Koziol, F.; Ochsenfeld, C.; Klärner, F.-G.; Spiess, H. W. *Angew. Chem., Int. Ed.* **2001**, *40*, 717−720.

(14) (a) Ochsenfeld, C. *Phys. Chem. Chem. Phys.* **2000**, *2*, 2153−2159. (b) Ochsenfeld, C.; Brown, S. P.; Schnell, I.; Gauss, J.; Spiess, H. W. *J. Am. Chem. Soc.* **2001**, *123*, 2597−2606.

methane molecule) were computed. The values obtained from these calculations agree very well with the predictions extracted from the NICS map, in which the explicit interaction between the phenol ring and neighboring atoms is neglected. We estimate the error due to this approximation to be of the order of 0.2 ppm at distances larger than 2.5 Å, of interest here.

Further, we investigated the impact of using the CPMD code, which is based on a pseudopotential plane wave scheme, and the neglect of dispersion interactions. For this purpose, we compared the CPMD NMR chemical shifts of the methane−benzene system in several representative geometries with all-electron DFT/BLYP and MP2 calculations done with the Gaussian package.[15] We used the 6-311++G** basis set for the DFT calculations and 6-311G** for MP2. It turns out that the difference between CPMD/BLYP and Gaussian/BLYP is of the order of 0.1 ppm, and the neglection of correlation results in an error of less than 0.3 ppm. Together with the error discussed above, we arrive at a maximum error margin of 0.6 ppm from the calculations, which corresponds to a maximum deviation of about 0.3 Å in space, as gradient of the NICS map is typically 0.5 Å per ppm.

These systematic errors of about 0.3 Å in total are smaller than the overall uncertainties of the approach. One limiting factor of distance constraints derived in this way is the nonuniqueness of ring-current effects: a given shift displacement could be caused by a single phenyl ring as well as by two phenyl rings with the same orientation at a larger distance (about 1.5 times larger). This slightly reduces the accuracy of distance constraints that can be derived from $\pi$-shifts, but they still contain significant information, so that the principal approach is not affected. Moreover, in the context of the dendritic systems studied here, it should also be noted that there is a dynamical component: The shift displacement can be averaged by rapid molecular motions, through which the spin experiences different frequency shifts.

Nevertheless, within a given scenario, shift effects on $^1$H resonances can reliably be used to locate protons relative to a phenyl ring in a distance range of 2−3 Å with an accuracy of ∼0.5 Å.

**2.3. Homo- and Heteronuclear Recoupling Pulse Sequences.** While the above-mentioned techniques are required for dipolar **de**coupling and for providing spectral resolution on the one hand, dipolar **re**coupling approaches are used on the other hand to gain access to information about molecular structure and dynamics, which is inherent to dipole−dipole couplings. By applying rotor-synchronized radio frequency (RF) pulse sequences, it is possible to compensate for the effect of sample rotation by a "counter-rotation" in spin space and, thus, to selectively reintroduce homo- or heteronuclear dipole−dipole couplings during specific periods of the NMR experiment. A method using homonuclear $^1$H−$^1$H couplings is two-dimensional $^1$H−$^1$H double-quantum MAS spectroscopy[16] (see Figure 3a),

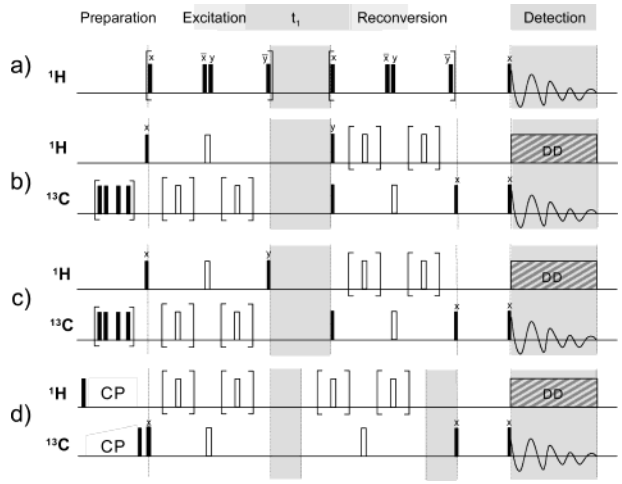


***Figure 3.*** Schematic representation of the 2D NMR experiments and pulse sequences applied in this study: (a) $^1$H−$^1$H DQ MAS spectroscopy, (b) $^1$H−$^{13}$C REPT-HSQC, (c) $^1$H−$^{13}$C REPT-HDOR, and (d) $^1$H−$^{13}$C REREDOR.

where the creation of a double-quantum (DQ) coherences between two protons relies on the existence of a sufficiently strong dipole−dipole coupling between them. Conversely, spatial proximities of protons can be directly inferred from the observed DQ signals. Under fast MAS conditions, a straightforwardly applicable recoupling scheme for $^1$H−$^1$H DQ spectroscopy is the so-called "back-to-back" (BABA) pulse sequence[16] (Figure 3a). Heteronuclear dipole−dipole couplings can be robustly and efficiently recoupled by trains of RF $\pi$-pulses, which is known as the REDOR (rotational-echo double-resonance) approach.[17]

In our NMR experiments, REDOR-type recoupling is used as a building block of different two-dimensional $^1$H−$^{13}$C experiments: (i) REPT-HSQC,[18] (ii) REPT-HDOR,[18] and (iii) REREDOR[19] (schematically displayed in Figure 3b−d). In these acronyms, REPT stands for recoupled polarization transfer, which is in our case a $^1$H→$^{13}$C transfer. HSQC and HDOR stand for heteronuclear single quantum correlation and heteronuclear dipolar order, respectively. REREDOR is a rotor-encoded REDOR technique. Further details about these NMR experiments will be given in the following.

In a HSQC experiment, $^1$H and $^{13}$C resonances are correlated in a two-dimensional fashion and the recoupling conditions can be chosen to cover only short-range or also longer-range C−H interactions. In the former case, only signals of $^1$H−$^{13}$C pairs with a direct chemical bond are observed in the spectra, while the latter case also allows for $^1$H→$^{13}$C polarization transfer to carbons without directly attached protons. In addition, due to the $^{13}$C chemical-shift dimension, HSQC spectra enable the distinction and the assignment of proton resonances which overlap in 1D $^1$H spectra. Skipping the $^1$H dimension of the HSQC experiment (Figure 3b) yields the TEDOR experiment,[20] which is particularly useful for obtaining a qualitative idea about the mobility of $CH_2$ groups. The $^{13}$C signal of rigid $CH_2$ groups disappears for recoupling times ($\tau_{rcpl}$) of two or more rotor

(15) Frisch, M. J.; Trucks, G. W.; Schlegel, H. B.; Scuseria, G. E.; Robb, M. A.; Cheeseman, J. R.; Zakrzewski, V. G.; Montgomery, J. A., Jr.; Stratmann, R. E.; Burant, J. C.; Dapprich, S.; Millam, J. M.; Daniels, A. D.; Kudin, K. N.; Strain, M. C.; Farkas, O.; Tomasi, J.; Barone, V.; Cossi, M.; Cammi, R.; Mennucci, B.; Pomelli, C.; Adamo, C.; Clifford, S.; Ochterski, J.; Petersson, G. A.; Ayala, P. Y.; Cui, Q.; Morokuma, K.; Malick, D. K.; Rabuck, A. D.; Raghavachari, K.; Foresman, J. B.; Cioslowski, J.; Ortiz, J. V.; Baboul, A. G.; Stefanov, B. B.; Liu, G.; Liashenko, A.; Piskorz, P.; Komaromi, I.; Gomperts, R.; Martin, R. L.; Fox, D. J.; Keith, T.; Al-Laham, M. A.; Peng, C. Y.; Nanayakkara, A.; Gonzalez, C.; Challacombe, M.; Gill, P. M. W.; Johnson, B.; Chen, W.; Wong, M. W.; Andres, J. L.; Gonzalez, C.; Head-Gordon, M.; Replogle, E. S.; Pople, J. A. *Gaussian 98*, Revision A.7; Gaussian, Inc.: Pittsburgh, PA, 1998.

(16) Schnell, I.; Spiess, H. W. *J. Magn. Reson.* **2001**, *151*, 153−227.
(17) (a) Gullion, T.; Schaefer, J. *J. Magn. Reson.* **1989**, *81*, 196−200. (b) Guillon, T. *Magn. Reson. Rev.* **1997**, *17*, 83−131.
(18) Saalwächter, K.; Graf, R.; Spiess, H. W. *J. Magn. Reson.* **2001**, *148*, 398−418.
(19) Saalwächter, K.; Schnell, I. *Solid-State Nucl. Magn. Reson.* **2002**, *22*, 154−187.
(20) Hing, A. W.; Vega, S.; Schaefer, J. *J. Magn. Reson.* **1992**, *96*, 205−209.

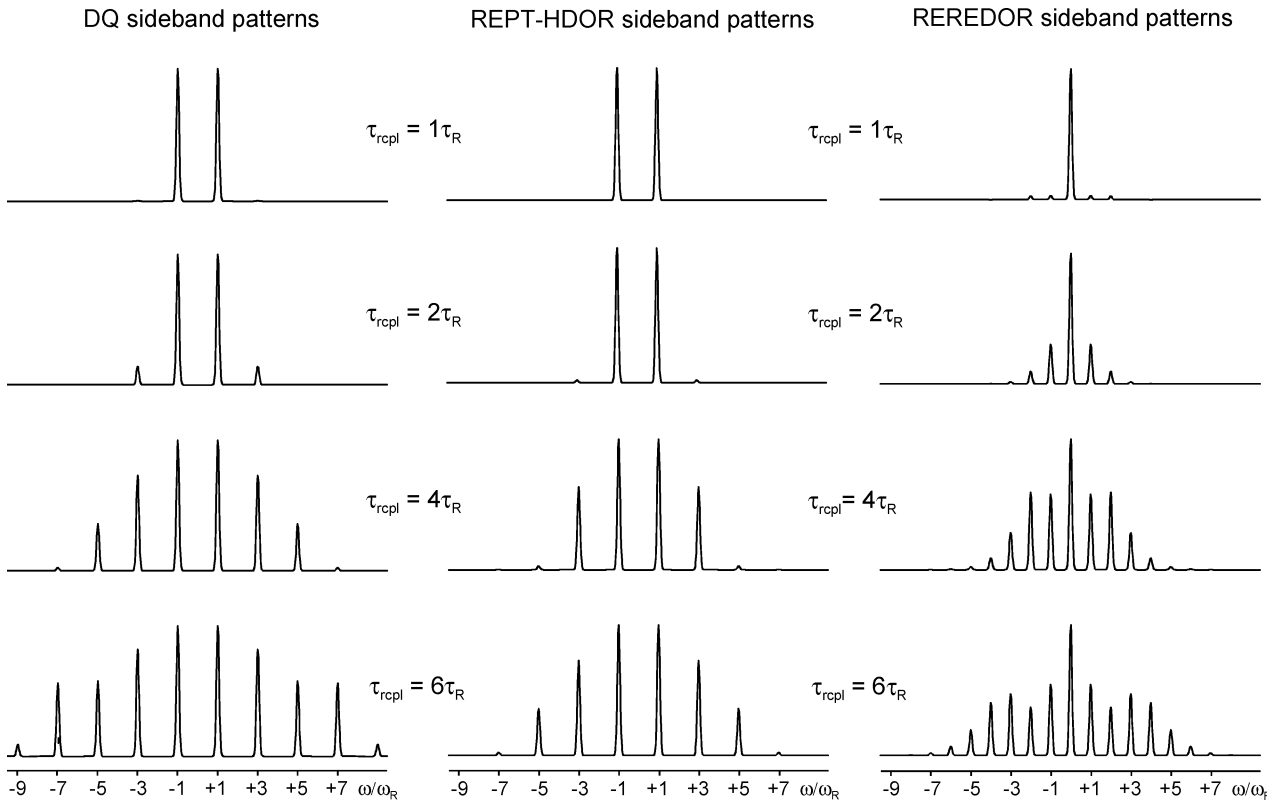


***Figure 4.*** Spinning sideband patterns of homonuclear DQ and heteronuclear REPT-HDOR and REREDOR experiments, calculated for a dipolar coupling ($D_{ij}$) of 10 kHz and different recoupling times ($\tau_{rcpl}$) under a MAS frequency of 30 kHz (corresponding to a rotor period of $\tau_R = 33.3$ $\mu$s).

periods ($\tau_{rcpl} \geq 2\tau_R$) at MAS frequencies $\geq$25 kHz.[21] Dynamic processes, however, may lead to an orientational averaging and, thus, to a motional reduction of the C−H dipole−dipole couplings in the $CH_2$ group, which is then reflected in the spectra by the reappearance of the respective $^{13}$C resonance for $\tau_{rcpl} \geq 2\ \tau_R$. Effectively, $^1$H−$^{13}$C TEDOR spectra of this type straightforwardly provide semiquantitative information of the local mobilities of $CH_2$ groups.

**2.4. Rotor-Encoded MAS Sideband Patterns.** In contrast to the REPT-HSQC experiment discussed above, the REPT-HDOR and REREDOR experiment do not correlate the chemical shifts of $^1$H and $^{13}$C resonance lines but rather aim at a sensitive and site-selective determination of the C−H dipole−dipole couplings by correlating the coupling information with the $^{13}$C chemical shifts. In REPT-HDOR and REREDOR experiments, C−H dipole−dipole couplings are measured by means of spinning sideband patterns, which arise in the indirect dimension as a result of the rotor-encoding of the recoupled dipolar interaction.[18,19] This rotor-encoding is introduced when the $t_1$ evolution time is incremented in fractions of a rotor period. In this way, the two average Hamiltonians representing the recoupling periods before and after $t_1$ effectively differ by an amplitude factor $\propto \bar{D}_{ij} \cos(\omega_R t_1)$, where $\bar{D}_{ij}$ and $\omega_R$ denote the (motionally reduced) C−H dipole−dipole coupling constant and the MAS frequency, respectively. Accordingly, the $^{13}$C signal intensities are modulated along $t_1$, and Fourier transformation yields a pattern of MAS-induced sidebands along the F1 frequency axis (Figure 4).

The distribution of the sideband intensities over the pattern is determined by the product of the recoupling time and the strongest C−H dipole−dipole coupling experienced by the $^{13}$C nuclei of interest. Hence, for a given C−H coupling, different recoupling times result in different spinning sideband patterns, with a longer excitation time generating higher-order sidebands (Figure 4). By relating the measured (residual) C−H couplings to those of a rigid C−H site, motional reduction factors can be determined individually for all $CH_n$ groups resolved in the $^{13}$C spectral dimension. The dipole−dipole coupling of an immobile segment, such as CH, $CH_2$, $CH_3$, or a phenyl ring, is known from both experiments and calculations. In our work, a coupling of $D_{CH}/2\pi = 20.4$ kHz is used, corresponding to a C−H bond length of 114 pm.[13,18,19,21]

For a $^1$H−$^{13}$C spin pair, the rotor-encoded signal observed in the $t_1$ dimension of REPT-HDOR and REREDOR experiments can be described by the following equations, which have been derived previously[18,19]

$$\text{REPT-HDOR:}\quad S(t_1) \propto \langle \sin N_{exc}\phi_0 \sin N_{rec}\phi_{t1} \rangle \tag{1}$$

$$\text{REREDOR:}\quad S(t_1) \propto \langle \sin N_{exc}\phi_0 \sin N_{rec}\phi_{t1} \rangle + \langle \cos N_{exc}\phi_0 \cos N_{rec}\phi_{t1} \rangle \tag{2}$$

The brackets $\langle\rangle$ denote the powder average, and $N_{exc}$ and $N_{rec}$ give the numbers of rotor periods, during which a recoupling pulse sequence is applied before (excitation, $\tau_{exc}$) and after (reconversion, $\tau_{rec}$) the $t_1$ dimension, respectively: $\tau_{exc} = N_{exc}\tau_R$ and $\tau_{rec} = N_{rec}\tau_R$. The phase angles, $\phi_0$ and $\phi_{t1}$, contain the dipole−dipole coupling $D_{ij}$, the orientation of the internuclear C−H vector in a rotor-fixed reference frame (in polar angles $\beta$ and $\gamma$), and the rotor modulation $\omega_R t_1$

(21) Fischbach, I.; Pakula, T.; Minkin, P.; Fechtenkötter, A.; Müllen, K.; Spiess, H. W.; Saalwächter, K. *J. Phys. Chem. B* **2002**, *106* (25), 6408−6418.

$$\phi_0 = \frac{-D_{ij}}{\omega_R} 2\sqrt{2} \sin 2\beta_{ij} \sin \gamma_{ij} \quad (3a)$$

$$\phi_{t1} = \frac{-D_{ij}}{\omega_R} 2\sqrt{2} \sin 2\beta_{ij} \sin(\omega_R t_1 + \gamma_{ij}) \quad (4a)$$

The sideband patterns resulting from Fourier transformation of $S(t_1)$ are shown in Figure 4. The same type of rotor encoding as in REPT-HDOR and REREDOR experiments can equally be introduced into REPT-HSQC and homonuclear $^1$H$-^1$H DQ MAS experiments by incrementing the $t_1$ dimension in steps $\Delta t_1 < \tau_R$, as mentioned above. In the $\omega_1$ dimension, the sideband patterns (REPT-HDOR type, as described by eq 1) are then shifted according to the chemical shifts of the $^1$H single-quantum or $^1$H$-^1$H double-quantum resonances in REPT-HSQC or $^1$H$-^1$H DQ experiments, respectively. For the rotor-encoded version of the REPT-HSQC, eqs 1, 3a, and 4a apply equally, while the phase angles, $\phi_0$ and $\phi_{t1}$, need to be scaled by a factor 3/2 for the $^1$H$-^1$H DQ sideband patterns due to different tensor scaling factors of homo- and heteronuclear interactions[16]

$$\phi_0' = \frac{-3D_{ij}}{\omega_R} \sqrt{2} \sin 2\beta_{ij} \sin \gamma_{ij} \quad (3b)$$

$$\phi_{t1}' = \frac{-3D_{ij}}{\omega_R} \sqrt{2} \sin 2\beta_{ij} \sin(\omega_R t_1 + \gamma_{ij}) \quad (4b)$$

In this way, $^1$H$-^1$H dipole−dipole couplings can be sensitively measured, which provides access to $^1$H$-^1$H internuclear distances or, in the case of a known distance, to motional order parameters for molecular segments. For example, the homonuclear coupling of two neighboring protons on a (rigid) phenyl ring with a distance of 247 pm[13] is $D_{HH}/2\pi = 8.0$ kHz. A noteworthy feature of these sideband patterns is that $^1$H$-^1$H DQ as well as $^1$H$-^{13}$C REPT patterns consist of only odd order sidebands, while REREDOR experiments generates odd and even order sidebands due to its mixed sine−cosine dependence (see eq 2). At first sight, more sidebands should mean a higher sensitivity of the pattern to the underlying dipole−dipole coupling, but practically more sidebands also mean that the signal is spread over more peaks, which reduces the overall signal-to-noise ratio. Essentially, the REREDOR experiment is advantageous when weak couplings or couplings of relatively rigid $CH_2$ groups need to be measured. In the latter case, the sine−sine dependence of the REPT signal (see eq 1) leads to signal cancellation for rigid $CH_2$ groups and recoupling times $\tau_{rcpl} > 60$ $\mu$s, as mentioned above.

## 3. Experimental Section

**Materials.** The dendritic macromolecules were synthesized via a controlled radical polymerization of the respective monodendrons. These in turn were obtained from polyhydroxymethyl benzoate building blocks.[7a,b] G1-PMA and G1-PS have $T_g$ values of ∼70 °C and G1-4EO-PMA of 5 °C (second heating). All three macromolecules form a hexagonal columnar liquid crystalline phase above their glass transition temperature. The isotropic phase of G1-PMA and G1-PS is reached at ∼130 °C and for G1-4EO-PMA at 105 °C. G2-PMA neither undergoes a glass transition nor a melting process before it decomposes at 250 °C. All investigations presented here have been performed below

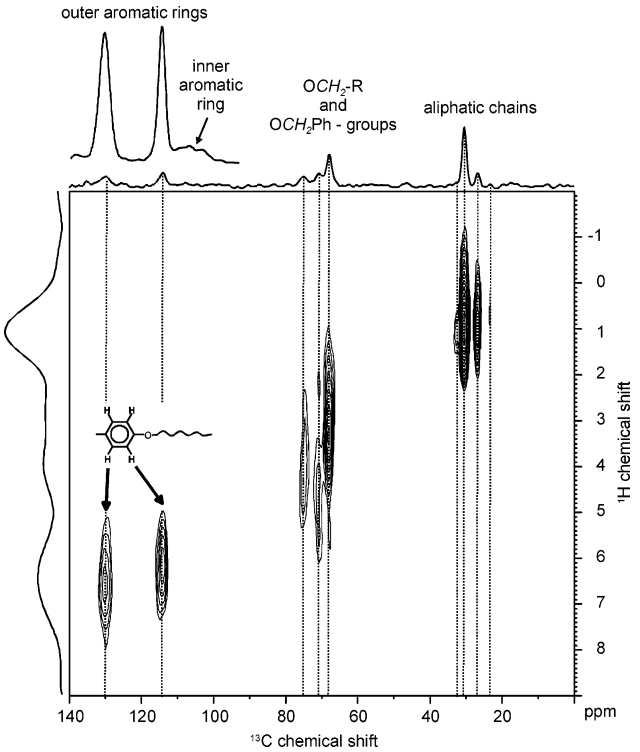


***Figure 5.*** 2D $^1$H$-^{13}$C REPT-HSQC correlation spectrum of G1-PMA, obtained at 25 kHz MAS using short dipolar recoupling periods of $\tau_{rcpl} = \tau_R = 40$ $\mu$s. The one-dimensional spectra plotted at the top and the left are the sum projections for the carbon and proton dimension, respectively.

$T_g$ of the respective material (G2-PMA has been studied at the same temperature as G1-PMA).

**NMR.** All solid-state data was collected on a Bruker DRX spectrometer with a 16.4 T magnet, operating at $^1$H and $^{13}$C Larmor frequencies of 700 and 176 MHz, respectively. A double-resonance MAS probe supporting rotors of 2.5 mm outer diameter allowed the experiments to be performed at MAS frequencies of 25 or 30 kHz. The $\pi/2$ radio frequency pulses were set to lengths of 2 $\mu$s, and a recycle delay of 1 s was used. The spectra are referenced to adamantane (1.63 ppm for $^1$H and 38.5 ppm for $^{13}$CH). If not stated otherwise, the spectra were recorded at room temperature, which, in combination with fast MAS, results in effective sample temperatures of 39 and 48 °C (± 2 °C) due to frictional heating at spinning frequencies of 25 and 30 kHz, respectively. All dipolar recoupling experiments were carried out with equal excitation and reconversion times. For the rotor-synchronized $^1$H$-^{13}$C REPT-HSQC spectra, an excitation time equal to one rotor period was used. For the spinning sideband patterns (without chemical shift resolution), two full rotor periods were recorded in the indirect dimension, with the time increment set to 2.2 or 2.5 $\mu$s for 30 or 25 kHz, respectively.

## 4. Results and Discussion

**4.1. Structural Features of G1-PMA: 2D $^1$H$-^{13}$C Correlation Spectra.** Figure 5 shows the two-dimensional $^1$H$-^{13}$C-correlation spectrum, recorded using the REPT-HSQC experiment displayed in Figure 2b. It allows the resonances of the carbons and their attached protons to be assigned for the different $CH_n$ groups of G1-PMA. A comparison of selected solid-state chemical shifts with the corresponding solution-state values (in brackets) is given in Table 1. In the 2D HSQC spectrum,

***Table 1.*** $^1$H and $^{13}$C Chemical Shifts of G1-PMA from $^1$H−$^{13}$C REPT-HSQC Solid-State Correlation Spectra and Solution-State NMR (in brackets)

| | G1-PMA | | | |
|---|---|---|---|---|
| | $\delta^{13}$C [ppm] | | $\delta^1$H [ppm] | |
| | solid-state | solution-state[7a] | solid-state | solution-state[7a] |
| 4-O*CH*$_2$R | 67.8 | (69.1) | 3.4 | (3.8) |
| (COO)*CH*$_2$Ph | ∼67.8 | (67.7) | b | (4.7) |
| 3,5-O*CH*$_2$Ph | 70.6 | (70.4) | 2.3 | (4.7) |
| | | | 4.3 | (4.7) |
| | | | 5.5 | (4.7) |
| 4-O*CH*$_2$Ph | 75.0 | (76.1) | 4.4 | (4.7) |
| outer phenyl CH, ortho | 114.0 | (114.0-114.8) | 6.3 | (6.6) |
| outer phenyl CH, meta | 130.0 | (129.0-130.5) | 6.7 | (7.0) |
| inner phenyl CH | 109.0 | (109.0) | ?[a] | (6.6) |

[a] The achievable signal intensity is too low to reliably determine the $^1$H chemical shift. [b] The $^1$H resonance is concealed by the high-frequency wing of the 4-O*CH*$_2$R peak.

three regions can be distinguished: the aromatic, the $OCH_2$, and the aliphatic region. No peaks of quaternary carbons are observed, because the REPT-HSQC experiment, when performed with short recoupling times of $\tau_{rcpl} = \tau_R = 40\ \mu$s (at 25 kHz MAS), is selective for carbons that couple to a directly bonded proton.

In the aromatic region, two peaks are observed at 114 and 130 ppm, which belong to the three outer aromatic rings of the dendron, as indicated in the inset in Figure 5. The CH signal of the inner aromatic ring is expected at a $^{13}$C chemical-shift of $\delta(^{13}C) = 109$ ppm but was only observed as a very weak signal in a conventional cross-polarization (CP) MAS spectrum, which is plotted above the sum projection of the carbon dimension in Figure 5. Thus, no corresponding $^1$H chemical shift can be assigned for the inner aromatic rings, as from the rather broad shape of the $^{13}$C peak (covering a spectral range from 100 to 115 ppm) a similarly broad distribution of the $^1$H resonances is expected. In the $OCH_2$ region, different types of groups can be distinguished, corresponding to the molecular structure of G1-PMA (depicted in Figure 1A): $OCH_2R$ groups in the dodecyl chain (with $R = C_{11}H_{23}$), $OCH_2Ph$ between the phenyl rings, and a $(COO)CH_2Ph$ group that links the dendron to the polymer backbone. The latter, however, is not visible in our NMR spectra because it is of weak intensity and, moreover, is covered by the low-frequency wing of the 4-$OCH_2R$ peak. On the basis of symmetry considerations, the $OCH_2Ph$ groups in the 4-position of the phenyl ring can be expected to exhibit different properties than those in the 3- and 5-positions. Therefore, a distinction is made according to 4-O*CH*$_2$Ph (blue), 3,5-O*CH*$_2$Ph (red), while the 4-$OCH_2R$ groups are shown in green. The aliphatic region is dominated by the dodecyl chains of the dendron. However, this region is not of major interest in this study, as the aliphatic side chains do not play a significant role in the self-assembling process of the dendritic polymer.

For the structure and, in particular, the molecular dynamics of the dendritic side groups, the $OCH_2$ units play a central role, as they link the different moieties. Therefore, they deserve a more detailed consideration, and the respective region of the 2D REPT-HSQC spectrum is enlarged in Figure 6A.

Three different $^{13}$C resonances are observed at 67.8 (green), 70.6 (red), and 75.0 ppm (blue) and are assigned to the 4-$OCH_2R$, 3,5-$OCH_2Ph$, and 4-$OCH_2Ph$ groups, respectively, based on solution-state NMR data. The corresponding $^1$H resonances range from 2.3 to 5.5 ppm (Table 1) and deviate noticeably from their solution-state values. Such effects can be attributed to ring currents of nearby aromatic moieties, which have been discussed above (see section 2.2).

In Figure 6A, three $^1$H resonances can be differentiated, which are all correlated to the $^{13}$C peak at 70.6 ppm. Hence, the four protons of the two 3,5-$OCH_2Ph$ groups do not have the same chemical environment but experience ring-current effects to different degrees. In Figure 2, the low-frequency shift to 2.3 ppm (relative to a solution-state value of ∼4.7 ppm, i.e., $\Delta = -2.4$ ppm) can be explained by a phenyl ring located at a distance of (2.5 ± 0.5) Å above or below the respective proton, while the high-frequency shift to 5.5 ppm (corresponding to $\Delta = +0.8$ ppm) suggests that this proton is placed beside a phenyl ring at a distance of ∼3 Å (relative to the center of the ring). To interpret these observations, possible scenarios of $CH_2$ groups with $\pi$-shifted protons are considered in the following. Ignoring signal intensities, the simplest scenario would be represented by three types of $CH_2$ groups which differ in their $^1$H chemical shifts: $H^{(+)}-C-H^{(+)}$, $H^{(0)}-C-H^{(0)}$, $H^{(-)}-C-H^{(-)}$, where the superscripts (+), (0), and (−) denote high-frequency shift, no shift, and low-frequency shift, respectively. While an unaffected group, $H^{(0)}-C-H^{(0)}$, can obviously be rationalized very easily, it is in fact unlikely that both protons of a $CH_2$ group are located relative to a phenyl ring in such a way that they are subject to equal ring currents at the same time, given the geometrical requirements and spatial restrictions for noticeable shift effects (see Figure 2). Therefore, $H^{(+)}-C-H^{(+)}$ and $H^{(-)}-C-H^{(-)}$ are unlikely situations. The combination of an up- and a downfield shifted proton on one $CH_2$ group, $H^{(+)}-C-H^{(-)}$, can also be excluded, because Figure 2 shows that the regions, where the ring current of a single phenyl ring would cause the observed shifts in both directions, are spatially separated by >2.5 Å. This distance is far too large for a single $CH_2$ group with a proton−proton distance of only 1.8 Å. Consequently, the $CH_2$ groups need to consist of a shifted ($H^{(+)}$ or $H^{(-)}$) and an unshifted proton ($H^{(0)}$), which leads us to two different types of $CH_2$ groups, namely, $H^{(+)}-C-H^{(0)}$ and $H^{(-)}-C-H^{(0)}$. This scenario also concurs with the observation that the peak at 4.3 ppm (i.e., $H^{(0)}$ with $\Delta \approx 0$ ppm) is stronger than the shifted ones at 2.3 ($H^{(-)}$) and 5.5 ppm ($H^{(+)}$).

Turning to the question which phenyl rings are responsible for the shifts, we first note that the observed effects cannot be caused by the phenyl rings attached to either side of the $-OCH_2-$ units alone. On the $OCH_2-Ph$ side, the effect is already included in the solution-state chemical shift, while on the $Ph-OCH_2$ side, the possible positions of the $OCH_2$ protons with respect to the phenyl ring allow for a $\pi$-shift effect of only 0 ppm $\leq \Delta \leq +0.2$ ppm, which is significantly less than the observed $\Delta = +0.8$ ppm.

Thus, we attribute the shift effects to phenyl rings of other dendrons (or other segments of the same dendron, but this possibility will be excluded later) which are arranged next to the 3,5-$OCH_2Ph$ groups according to the two distance constraints derived above (see also Figure 12b below): (i) a neighboring phenyl ring is located above or below one of the two 3,5-$OCH_2Ph$ groups such that one of its two protons points toward the center of the ring ("face-on"-type arrangement); (ii) the other 3,5-$OCH_2Ph$ group is oriented such that one of its protons is placed at a distance of ∼3 Å beside another phenyl

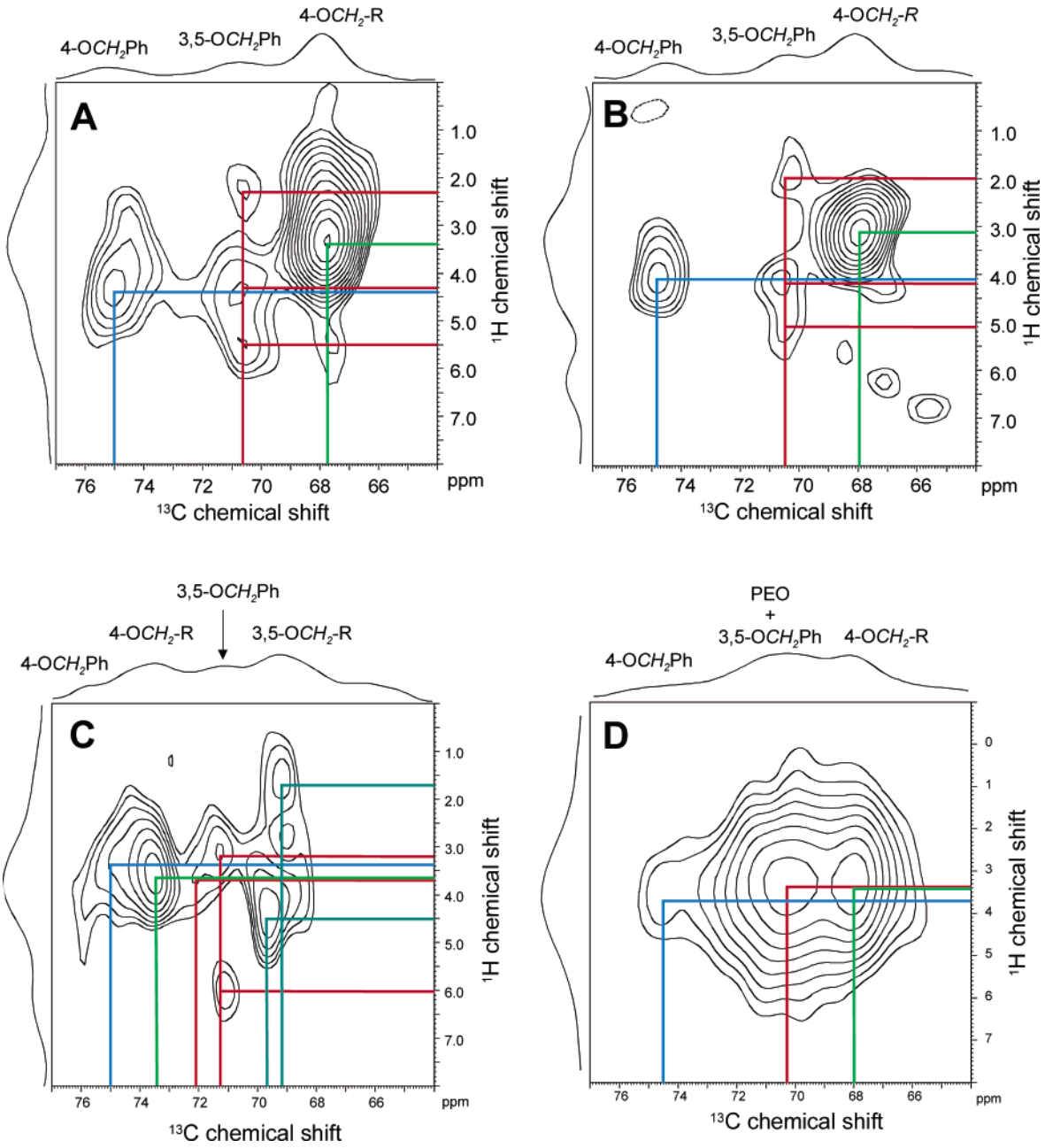


***Figure 6.*** $OCH_2$ region of 2D $^1H-^{13}C$ REPT-HSQC correlation spectra obtained under MAS at 25−30 kHz using $\tau_{rcpl} = \tau_R$: (**A**) G1-PMA, (**B**) G1-PS, (**C**) G2-PMA, and (**D**) G1-4EO-PMA.

ring ("edge-on"-type arrangement). In both cases, only one of the two $CH_2$ protons experiences additional ring currents, while the other proton remains essentially unaffected. Finally, from the observation of three distinct chemical shifts, it is evident that the 3,5-$OCH_2$Ph groups are rather immobile on the NMR time scale (i.e., 10 $\mu$s to 1 ms) so that the $^1H$ chemical shifts are not motionally averaged. The presence of only one (average) $^1H$ chemical shift of the 4-$OCH_2$Ph groups, however, can be attributed to motional effects. We will return to this point in the discussion of $CH_2$ dynamics below, where the structural features derived above will be combined with features of segmental motion.

**4.2. Segmental Dynamics of G1-PMA: $^1H-^{13}C$ and $^1H-^1H$ Sideband Patterns.** Turning to the molecular dynamics of G1-PMA, qualitative information can be straightforwardly obtained from one-dimensional $^1H-^{13}C$ TEDOR spectra recorded with a recoupling time of $\tau_{rcpl} \geq 2\ \tau_R$ for MAS frequencies of 25−30 kHz (as described above), because under these experimental conditions the $^{13}C$ signal of immobile $CH_2$ groups vanishes. Considering the $OCH_2$ groups of G1-PMA, only the peak at 71 ppm disappears; therefore, only the 3,5-$OCH_2$Ph groups are largely rigid (Figure 7A). For $\tau_{rcpl} = 4\tau_R$, the 4-$OCH_2$Ph group disappears too; obviously, it fulfils the condition for signal cancellation at longer recoupling times due to weaker dipole−dipole couplings. Therefore, it must be a little more mobile than the 3,5-$OCH_2$Ph groups but still a lot less mobile than the 4-$OCH_2$R groups in the alkyl chains, as their signal at 68 ppm clearly persists at $\tau_{rcpl} = 4\tau_R$.

To extend this qualitative understanding to a quantitative measurement, the segmental dynamics can be determined by means of spinning sideband patterns which arise from heteronuclear ($^1H-^{13}C$) or homonuclear ($^1H-^1H$) dipole−dipole

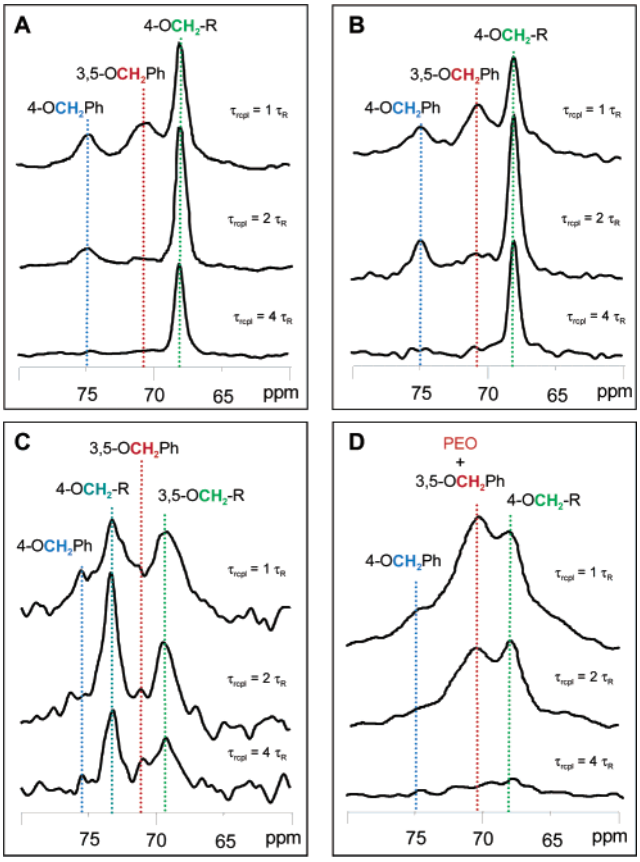


***Figure 7.*** $OCH_2$ region of one-dimensional $^1H-^{13}C$ TEDOR spectra of (**A**) G1-PMA, (**B**) G1-PS, (**C**) G2-PMA, and (**D**) G1-4EO-PMA recorded under MAS at 30 kHz.

couplings according to the rotor-encoding mechanisms described above (eqs 1−4). According to conventional definitions, a dynamic order parameter $S$ can be determined locally for individual segments by relating the measured (reduced) coupling and that of the immobile case. Effectively, the parameter $S$ reflects the motion of the internuclear vector (C−H or H−H) in terms of its reorientation with respect to the external magnetic field vector $B_0$. Recalling the cancellation effects observed in $^1H-^{13}C$ TEDOR spectra, it should be noted that $^1H-^{13}C$ REPT experiments and their sideband patterns are not suited for measuring couplings of relatively rigid $CH_2$ groups, because the 2D REPT sequences are extended versions of the TEDOR experiment and therefore equally suffer from signal losses. Instead, rigid $CH_2$ groups are investigated by REREDOR experiments and their sideband patterns.

When fitting REPT-HDOR and DQ sideband patterns, the first-order sidebands are neglected, because their intensity is usually too high due to couplings to remote protons.[18] Similarly, the center band of REREDOR sideband patterns is excluded from the evaluation as its intensity is strongly affected by relaxation processes.[19] The error margin of the residual dipolar couplings extracted from the relative intensities of the sidebands predominantly depends on the signal-to-noise ratio of the experiment. For the REPT-HDOR and DQ sideband patterns shown below, it can be estimated to be about $\Delta D_{ij}/2\pi \approx 0.5$ kHz. In REREDOR experiments, the signal is spread over a larger number of sidebands and, in addition, the patterns are a little less sensitive to the coupling, such that the REREDOR

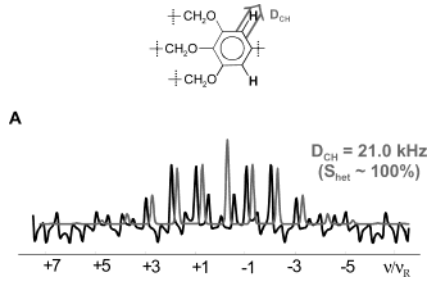


***Figure 8.*** Residual dipolar $^1H-^{13}C$ coupling of the inner phenyl rings of (**A**) G1-PMA measured by a REREDOR spinning sideband pattern recorded under MAS at 30 kHz and applying $\tau_{rcpl} = 2\ \tau_R = 67\ \mu s$ (black line = experimental, gray line = calculated). The coupling vector is indicated in the inset above.

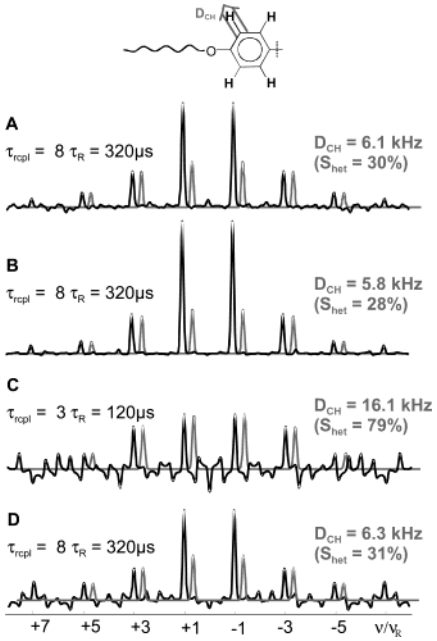


***Figure 9.*** Residual $^1H-^{13}C$ dipolar couplings of the outer phenyl rings of (**A**) G1-PMA, (**B**) G1-PS, (**C**) G2-PMA, and (**D**) G1-4EO-PMA, as measured by REPT-HDOR spinning sideband patterns recorded under MAS at 25 kHz and applying the recoupling times given in the figure (black line = experimental, gray line = calculated).

error margin is effectively about twice as large, i.e., $\Delta D_{ij}/2\pi \approx 1.0$ kHz.

For G1-PMA, Figures 8 and 9A show $^1H-^{13}C$ REREDOR and REPT-HDOR patterns of CH groups of the inner and outer aromatic rings, respectively. Figure 10A depicts the $^1H-^1H$ DQ sideband patterns for the outer aromatic rings, while the REREDOR sideband patterns of the $OCH_2$ groups are shown in Figure 11. These results are discussed below.

*Motions of Aromatic Rings*. The inner aromatic ring of the dendrons is fully immobile, while the outer ones are significantly mobile. Comparing Figures 8 and 9A, the best fit for the sideband pattern of the inner and outer aromatic ring gives heteronuclear couplings of $D_{CH}/2\pi = 21.0$ and 6.1 kHz, corresponding to order parameters of $S_{het} \approx 100\%$ and 30%, respectively. For the outer aromatic rings, the homonuclear coupling between the two neighboring aromatic protons can be measured too, where a coupling of $D_{HH}/2\pi = 4.9$ kHz, corresponding to $S_{hom} = 61\%$, is determined (Figure 10A).

For phenyl rings, the comparison of homo- and heteronuclear dipolar couplings is informative because only the heteronuclear

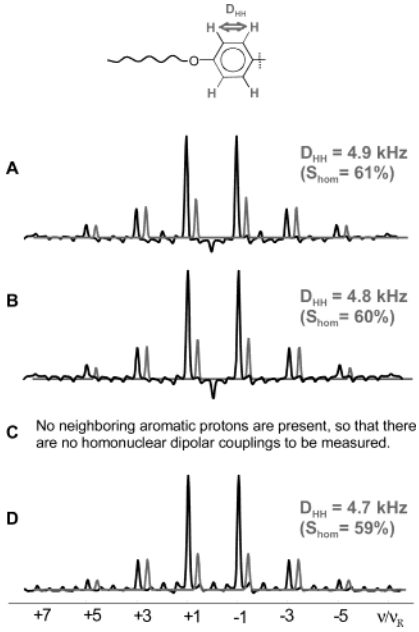


***Figure 10.*** Residual $^1$H−$^1$H dipolar coupling of outer phenyl rings of (**A**) G1-PMA, (**B**) G1-PS, and (**D**) G1-4EO-PMA, as measured by DQ sideband patterns recorded under MAS at 30 kHz and applying $\tau_{rcpl} = 8\ \tau_R = 267$ $\mu$s, (black line = experimental, gray line = calculated).

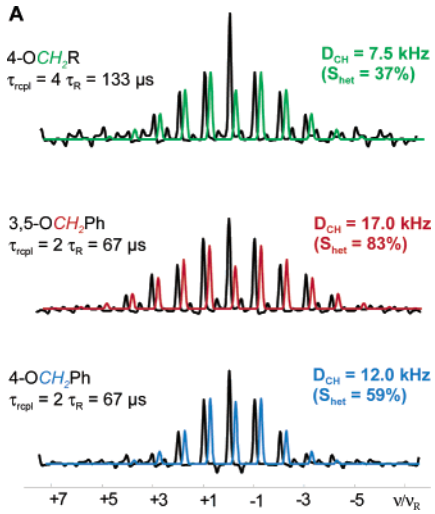


***Figure 11.*** Residual $^1$H−$^{13}$C dipolar couplings of the different $OCH_2$ groups of (**A**) G1-PMA, as measured by REREDOR spinning sideband patterns recorded under MAS at 30 kHz and applying the recoupling times given in the figure (black lines = experimental, colored lines = calculated).

coupling is affected by a flip or a rotation of the aromatic rings.[21] The homonuclear coupling between the two aromatic protons remains unaffected by a flip or rotation because the dipolar coupling vector lies parallel to the flip/rotation axis. Therefore, a reduction of the homonuclear coupling must be due to a motion of the whole side chain, while the heteronuclear dipolar coupling can be reduced by both, the side chain movement and a local ring flip. The reduced homonuclear coupling ($D_{HH}/2\pi$ = 4.9 kHz, $S_{hom}$ = 61%) can be related to a side chain motion which effectively occurs within a cone-shaped volume with an opening angle of ±20° (see below, Figure 12a). The angular restriction can be estimated directly from the residual order parameter $S_{hom} \approx 60\%$.[23]

In the heteronuclear experiment, a lower order parameter of $S_{het}$ = 30% is found, which indicates a phenyl ring flip that occurs in addition to the side chain motion. A pure 180° flip would result in an order parameter of $S_{het}$ = 63% for the C−H coupling.[24] When flip and side chain motions are considered independent of each other, the effective heteronuclear order parameter can be calculated according to $S_{het} = S_{hom} \times 63\% = 38\%$, which would correspond to $D_{CH}/2\pi = 7.8$ kHz (see Table 2). These numbers are slightly higher than experimental ones ($D_{CH}/2\pi$ = 6.1 kHz, $S_{het}$ = 30%), which points at a liberating small-angle motion of the aromatic rings on top of the 180° ring flip. However, a full ring rotation can be excluded, because the resulting coupling would then be much lower ($D_{CH}/2\pi$ = 2.6 kHz, $S_{het}$= 13%)[24] than the experimental one, not even taking into account the side chain motion. These results show very clearly that there is a pronounced mobility gradient among the aromatic residues of the dendron with order parameters changing from 100% to 61% (30% including the flip) between the inner and outer aromatic rings.

***Table 2.*** Experimental and Calculated Residual Dipolar Couplings for the Possible Motions of the Outer Aromatic Rings in G1-PMA

| | calculated/**experimental** couplings and order parameters | |
|---|---|---|
| | homonuclear H–H $D_{HH}/2\pi$ ($S_{hom}$) | heteronuclear C-H $D_{CH}/2\pi$ ($S_{het}$) |
| rigid aromatic ring | 8.0 kHz[a] (100%) | 20.4 kHz[b] (100%) |
| 180° ring flip | 8.0 kHz (100%) | 12.8 kHz (63%) |
| full ring rotation | 8.0 kHz (100%) | 2.6 kHz (13%) |
| only chain motion | **4.9 kHz (61%)** | →12.4 kHz (61%) |
| chain motion plus 180° ring-flip | | →7.8 kHz (38%), **6.1 kHz (30%)** |

[a] Calculated using $r_{HH}$ = 2.47 Å.[13] [b] Calculated using $r_{CH}$ = 1.14 Å.[18,19,21]

***Table 3.*** Residual Dipolar $^1$H−$^{13}$C Couplings of $OCH_2$ Groups of G1-PMA from REREDOR Experiments

| | heteronuclear C-H $D_{CH}/2\pi$ ($S_{het}$) |
|---|---|
| 4-$OCH_2$R | 7.5 kHz (37%) |
| 3,5-$OCH_2$Ph | 17.0 kHz (83%) |
| 4-$OCH_2$Ph | 12.0 kHz (59%) |

*Motions of $OCH_2$ Groups.* In the qualitative study, it has already been noted that 4-$OCH_2$R groups are significantly more mobile than the Ph$OCH_2$Ph groups (see Figure 7A). The residual dipolar couplings, as obtained from the REREDOR sideband patterns shown in Figure 11, are listed in Table 3. Since the $^{13}$C resonance lines of the 4-$OCH_2$Ph and 3,5-$OCH_2$Ph groups are separated, their mobility can be determined independently, confirming that the 4-$OCH_2$Ph segment is more mobile ($S_{het}$ = 59%) than the ones in positions 3 and 5 ($S_{het}$ = 83%). This effect is most likely due to steric hindrances from neighboring dendritic groups, which affect the chains in the 3- and 5-positions more severely. The extent to which this effect is also present for the outer aromatic rings and the attached 4-$OCH_2$R groups cannot be determined, because the chemical shifts can no longer be distinguished. Rather, the value of $S_{het}$ = 37% determined for 4-$OCH_2$R, as well as the values $S_{hom}$ = 61% and $S_{het}$ = 30% determined above for the phenyl rings, represent

(22) Discussion of internuclear distances as determined by NMR and alternative methods: (a) Ishii, Y.; Terao, T.; Soichi, H. *J. Chem. Phys.* **1997**, *107*, 2760−2774. (b) Case, D. A. *J. Biomol. NMR* **1999**, *15*, 95−102.
(23) (a) Schmidt-Rohr, K.; Spiess, H. W. *Multidimensional Solid-State-NMR and Polymers*; Academic Press: London, 1997. (b) Hentschel, R.; Sillescu, H.; Spiess, H. W. *Polymer* **1981**, *22*, 1516.
(24) Macho, V.; Brombacher, L.; Spiess, H. W. *Appl. Magn. Reson.* **2001,** *20*, 405−432. (http://www.mpip-mainz.mpg.de/weblab40/)

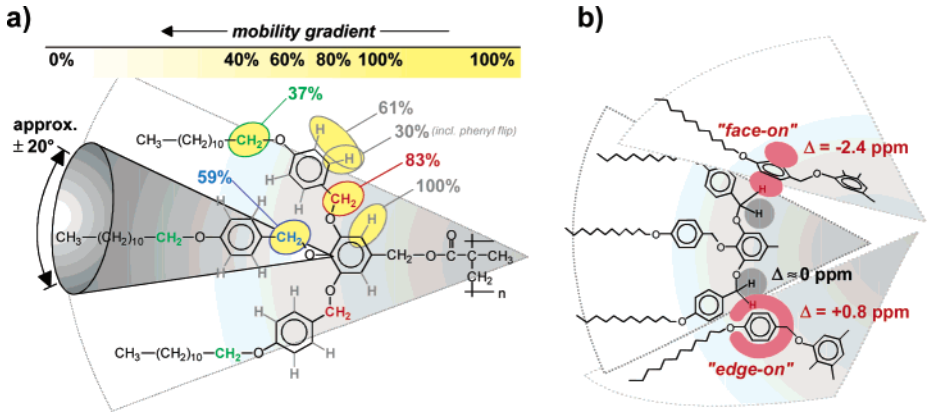


***Figure 12.*** Characteristic features of the molecular dynamics and packing of the dendrons in G1-PMA. (a) A mobility gradient along the dendrons is obvious from the local order parameters. On the basis of S ≈ 60%, the motion of the three linear chains occurs within a cone with an opening angle of approximately ±20°.[23] (b) From the $^1$H chemical-shift effects observed for the 3,5-$OCH_2$Ph groups, "face-on" and "edge-on" types of contacts between dendrons can be derived. The figure should only be taken as a schematic visualization of principal structural features rather than a part of the actual structure.

averages over all three rings. On the basis of the $OCH_2$Ph results, however, it can be assumed that the chain in the 4-position is more mobile, as a whole, than the other two chains.

On going from the outer phenyl rings ($S_{hom}$ = 61%) to the attached 4-$OCH_2$R groups ($S_{het}$ = 37%), the segmental mobility increases by a factor of ~1.6, which can only be attributed to a liberating effect of the −O− segment between the phenyl ring and the $CH_2$ group. A similar effect is also observed when comparing the inner aromatic ring and the attached $OCH_2$Ph groups. Correspondingly, the −O− segment leads to an increase in the segmental mobility by factors of 1.2−1.7.

*Structural Implicatons from NMR Data*. Figure 12 schematically summarizes the various pieces of information which have been gained so far about the structure, dynamics, and packing of the dendrons in G1-PMA. The segmental dynamics (given in detail in Figure 12a) show a clear mobility gradient along the dendrons, ranging from the immobile inner phenyl rings to the mobile ends of the aliphatic chains. The order parameter of the terminating methyl groups at the alkyl chains could be estimated to $S < 4\%$ by means of REREDOR experiments with long recoupling times (results not shown). The order parameter $S \approx 60\%$ of the outer phenyl rings can be understood in terms of an angular motion by which the chain covers a cone-shaped volume with an opening angle of approximately ±20° (as indicated in Figure 12a).[23]

Combining the results on the molecular dynamics with the observed $^1$H chemical-shift effects (see section 4.1 and Table 1), some features of the dendron packing can be derived, which are depicted schematically in Figure 12b. A few conclusions concerning the structure of the dendrons and their packing have already been drawn in section 4.1, which are now to be completed by consideration of the segmental dynamics. As discussed above, the shift effects allow the $CH_2$ protons of the 3,5-$OCH_2$Ph groups to be located either above/below or beside a phenyl ring (according to $\Delta = -2.4$ or +0.8 ppm, respectively). The respective regions are relatively small and restricted (highlighted in red in Figure 12b), so that the phenyl ring causing the shifts has to be relatively immobile. Otherwise, motional averaging would lead to less pronounced shift effects. This kind of situation is observed in the case of the 4-$OCH_2$Ph groups, where a combination of $\Delta \approx 0$ ppm and $S = 59\%$ is found. Consequently, the phenyl rings belonging to the chains in the 4-position can hardly cause the $^1$H shift effects of the 3,5-$OCH_2$Ph groups.

Following the mobility argument, the inner and immobile phenyl ring needs to be considered for the $\pi$-shifts, but there is only one such inner phenyl ring per dendron and, in addition, there are considerable steric hindrances, in particular for the "edge-on"-type arrangement beside the phenyl ring. It cannot be excluded that the inner phenyl ring contributes to the $\Delta = -2.4$ ppm shift effect in the "face-on"-type arrangement, but it is most likely that the outer phenyl rings in the 3- and 5-positions of neighboring dendrons dominate the $^1$H shift effects of the 3,5-$OCH_2$Ph groups. Schematically, Figure 12b shows possible "edge-on" and "face-one" arrangements between dendrons, which would lead to the observed effects. At this point, however, a word of caution needs to be added. The features displayed in Figure 12b are derived from a combination of NMR results and should be taken as suggestions for *local* packing phenomena. These local features belong to an overall structure which can, as a whole, not be determined by NMR experiments alone. In particular, we do not know whether each dendron is involved in edge-on- and face-on-type arrangements at the same time or whether there are different types of dendrons packed in face-on, edge-on, and mixed arrangements.

**4.3. G1-PS vs G1-PMA.** G1-PS has the same dendritic side group as G1-PMA but attached to a polystyrene backbone instead of a polymethacrylate one. G1-PS self-assembles into a columnar structure similar to G1-PMA and also exhibits a hexagonal liquid crystalline phase above $T_g$. Comparing the local structure and dynamics of the two supramolecular systems provides insight into the role the polymer backbone plays in the self-assembly process of the columnar structure.

Figure 6B shows the $OCH_2$ region of the $^1$H−$^{13}$C REPT-HSQC spectrum of G1-PS. Comparing this spectrum to the one of G1-PMA (Figure 6A), similar $^1$H chemical shifts are observed, which indicates that similar $\pi$-shifts are present in both systems. This observation suggests that the inner $OCH_2$ groups and the outer aromatic rings arrange in a similar fashion in both systems. Consequently, the polymer backbone does not have a pronounced influence on the structure adopted by the

***Table 4.*** Residual Heteronuclear $^1H-^{13}C$ Couplings of G1-PS and G1-PMA from REPT-HDOR and REREDOR Spinning Sideband Patterns as Well as Residual Homonuclear $^1H-^1H$ Couplings from DQ Sideband Patterns

| | experimental couplings and order parameters | |
|---|---|---|
| | **G1-PS** heteronuclear C-H $D_{CH}/2\pi$ ($S_{het}$) | **G1-PMA** heteronuclear C-H $D_{CH}/2\pi$ ($S_{het}$) |
| inner aromatic ring | not measured | 21.0 kHz (~100%) |
| 3,5-$OCH_2$Ph | 16.0 kHz (78%) | 17.0 kHz (83%) |
| 4-$OCH_2$Ph | 13.0 kHz (64%) | 12.0 kHz (59%) |
| outer phenyl rings | 5.8 kHz (28%) | 6.1 kHz (30%) |
| *homonuclear H−H* $D_{HH}/2\pi$ ($S_{hom}$) | *4.8 kHz (55%)* | *4.9 kHz (56%)* |
| 4-$OCH_2$R | 7.0 kHz (34%) | 7.5 kHz (37%) |

system, which is rather driven by the steric requirements as well as the $\pi-\pi$ interactions of the dendron.

This conclusion is further supported by the local dynamics of the dendritic side groups of G1-PS. The $^1H-^{13}C$ TEDOR spectra (Figure 7B) as well as the REREDOR sideband patterns of the $OCH_2$ groups (not shown) prove that the dynamical properties of G1-PS are very similar to G1-PMA. Moreover, the residual dipole−dipole couplings and order parameters observed for the outer aromatic rings ($^1H-^{13}C$ and $^1H-^1H$ couplings in Figures 9B and 10B, respectively) are practically identical, too. The values are listed in Table 4. Thus, not only the local structure but also the dynamics of G1-PMA and G1-PS are largely identical despite the different polymer backbones.

**4.4. G2-PMA vs G1-PMA.** The G1-PMA and G1-PS systems discussed so far contain dendrons of the first generation. To study the influence of the generation on the supramolecular arrangement, the results obtained for G1-PMA shall now be compared to those for G2-PMA with a PMA backbone and dendritic side groups of second generation. In the solid phase, G2-PMA also self-assembles in a columnar structure, but neither a pronounced glass transition nor an isotropic phase is observed before the compound decomposes at 250 °C.

*Chemical Shifts*. A comparison of selected solid-state chemical shifts of G2-PMA with the corresponding solution-state values (in brackets) and the values of G1-PMA is given in Table 5. On the basis of the solution-state NMR data, the $^{13}C$ resonances between 69 and 75 ppm, as observed in the $^1H-^{13}C$ correlation spectrum (Figure 6C), could be assigned to the different $OCH_2$ groups. As mentioned above for G1-PMA and G1-PS, the 4-$OCH_2$Ph groups (blue in Figure 6C) are expected to have a different $^{13}C$ chemical shift than the 3,5-substituted ones (red in Figure 6C). Accordingly, G2-PMA, 4-$OCH_2$R (green), and 3,5-$OCH_2$R (dark green) are expected to have different $^{13}C$ chemical shifts. However, there are two more $^{13}C$ chemical shifts present: For the 3,5-$OCH_2$Ph and the 3,5-$OCH_2$R groups, pairs of resonances are observed (71.3/72.1 and 69.2/69.7 ppm, respectively). This could either mean that in G2-PMA the 3-$OCH_2$ and 5-$OCH_2$ groups have a slightly different environment or that the organization of the 3,5-$OCH_2$ groups is not fully identical throughout the macromolecule. With respect to the structure, however, the observation of more than one $^1H$ resonance for the 3,5-$OCH_2$ groups is more significant. Similar to G1-PMA, the 3,5-$OCH_2$Ph protons are found to be shifted due to aromatic ring currents to higher and lower frequencies, i.e., 6.0 and 3.2 ppm compared to the solution-state value of 4.8 ppm. On the basis of Figure 2, the shift

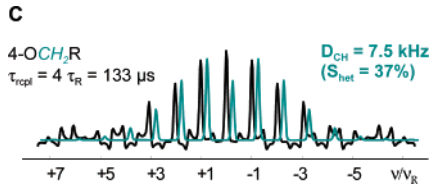


***Figure 13.*** Residual $^1H-^{13}C$ dipolar couplings of the $OCH_2R$ groups of (**C**) G2-PMA, as measured by REREDOR spinning sideband patterns recorded under MAS at 30 kHz (black line = experimental, green line = calculated).

changes of $\Delta = 1.2$ and $-1.6$ ppm can be converted to proton locations at distances of ~3 Å beside and (3.0 ± 0.5) Å above/below the center of a phenyl ring, respectively. In G2-PMA, the shifts tend to slightly higher frequencies than in G1-PMA, and all $OCH_2$Ph protons experience $\pi$-shifts of nearby aromatic rings, so that no chemical shift close to the solution-state value is observed. This can be attributed to the higher density of phenyl systems in G2-PMA. For the 3,5-$OCH_2$R groups, similar $\pi$-shifts lead to two different $^1H$ resonances at 4.5 and 1.7 ppm, compared to the solution-state value of 3.6 ppm (i.e., $\Delta = 0.9$ and $-1.9$ ppm). These values correspond to proton locations at distances of ~3 Å beside and (2.5 ± 0.5) Å above/below the center of a phenyl ring, respectively. These findings bear similarities to the 3,5-$OCH_2$Ph segments in G1-PMA, which points at a similar exposure of the 3,5-$OCH_2$ protons to nearby aromatic systems. From a structural point of view, 3,5-$OCH_2$Ph in G1-PMA and 3,5-$OCH_2$R in G2-PMA play a similar role in the dendrons, since both units link a linear side chain to a 3,4,5-substituted phenyl ring.

Considering the chemical shifts in G1- and G2-PMA, it is evident that the dendrons of first and second generation exhibit similar general features and can thus be expected to pack in a similar fashion. In G2-PMA, the local density of phenyl rings is obviously higher around the $OCH_2$ groups, which leads to more pronounced $\pi$-shift effects.

*Molecular Dynamics*. The dynamic properties of G2-PMA are different from G1-PMA, as will be discussed in the following. Starting with the outer phenyl rings, Figure 9C shows a $^1H-^{13}C$ REPT-HDOR sideband pattern from which a coupling of $D_{CH}/2\pi = 16.1$ kHz is determined, corresponding to $S_{het} = 79\%$. Hence, the outer aromatic rings in G2-PMA are a lot less mobile than in G1-PMA and G1-PS (where $S_{het} \approx 30\%$ and 60% with and without the phenyl flip, respectively). This is not too surprising because the outer rings in G2-PMA are centers of dendritic units (with a 3,4,5-substitution) while in G1-PMA the outer ring is only part of a linear side chain (only 4-substitution). Indeed, the coupling value of $D_{CH}/2\pi = 16.1$ kHz shows that the phenyl ring flip is inhibited, as such a flip would be associated with a reduction of the coupling to 12.8 kHz. In comparison to the inner ring in G1-PMA (with $S_{het} \approx 100\%$), however, the outer rings in G2-PMA are more mobile (with $S_{het} = 79\%$). This is because the outer rings in G2-PMA carry only linear alkyl side chains, but no phenyl rings which would be capable of $\pi-\pi$ stacking.

Turning to the alkyl side chains attached to the outer phenyl rings, the same couplings $D_{CH}/2\pi = 7.5$ kHz and order parameters $S_{het} = 37\%$ are found for the 4-$OCH_2$R groups in G1- and G2-PMA (see Figures 11 and 13). Thus, the dynamics of these $CH_2$ groups appears to be dominated by the dynamics of the alkyl chain rather than by the inner part of the dendron.

***Table 5.*** $^1$H and $^{13}$C Chemical Shifts of G1-PMA and G2-PMA from $^1$H−$^{13}$C REPT-HSQC Solid-State Correlation Spectra and Solution-State NMR (in brackets)

| | **G1-PMA** solid (solution-state) | | **G2-PMA** solid (solution-state) | |
|---|---|---|---|---|
| | $\delta(^{13}C)$ [ppm] | $\delta(^1H)$ [ppm] | $\delta(^{13}C)$ [ppm] | $\delta(^1H)$ [ppm] |
| 3,5-$OCH_2$R | *a* | *a* | 69.2 (68.5) | 1.7 (3.6) |
| | *a* | *a* | 69.7 (68.5) | 4.5 (3.6) |
| 4-$OCH_2$R | 67.8 (69.1) | 3.4 (3.8) | 73.5 (73.1) | 3.7 (3.8) |
| 3,5-$OCH_2$Ph | 70.6 (70.4) | 2.3 (4.7) | 71.3 (71.2) | 3.2 (4.9) |
| | | 4.3 (4.7) | | 6.0 (4.9) |
| | | 5.5 (4.7) | 72.1 (71.3) | 3.7 (4.9) |
| 4-$OCH_2$Ph | 75.0 (76.1) | 4.4 (4.7) | 75.0 (74.8) | 3.4 (4.8) |
| outer phenyl CH, ortho | 114.0 (114.0-114.8) | 6.3 (6.6) | 106.0 (105.7-106.3) | 6.4 (6.5) |
| outer phenyl CH, meta | 130.0 (129.0-130.5) | 6.7 (7.0) | *a* | *a* |
| inner phenyl CH | 109.0 (109.0) | ?[b] (6.6) | 110.0 (110.1) | ?[b] (6.7) |

[a] No such group is present in the molecule. [b] The signal intensity in the 2D REPT-HSQC spectrum is too low to reliably determine the $^1$H chemical shift.

***Table 6.*** $^1$H and $^{13}$C Chemical Shifts of G1-PMA and G1-4EO-PMA from $^1$H−$^{13}$C REPT-HSQC Solid-State Correlation Spectra and Solution-State NMR (in brackets)

| | **G1-PMA** solid (solution) | | **G1-4EO-PMA** solid (solution) | |
|---|---|---|---|---|
| | $\delta(^{13}C)$ [ppm] | $\delta(^1H)$ [ppm] | $\delta(^{13}C)$ [ppm] | $\delta(^1H)$ [ppm] |
| 4-$OCH_2$R | 67.8 (69.1) | 3.4 (3.8) | 68.0 (68.1) | 3.5 (3.9) |
| 3,5-$OCH_2$Ph | 70.6 (70.4) | 2.3 (4.7) | 70.3 (71.3) | 3.5 (5.0) |
| | | 4.3 (4.7) | | |
| | | 5.5 (4.7) | | |
| 4-$OCH_2$Ph | 75.0 (76.1) | 4.4 (4.7) | 74.5 (74.8) | 3.7 (5.0) |
| -$(OCH_2CH_2)_4$- linker | *a* | *a* | 70.3 (70.8) | 3.5 (3.6) |
| outer phenyl CH, ortho | 114.0 (114.0-114.8) | 6.3 (6.6) | 114.0 (114.0-114.6) | 6.1 (6.7-6.9) |
| outer phenyl CH, meta | 130.0 (129.0-130.5) | 6.7 (7.0) | 130.7 (129.4-130.3) | 6.6 (7.2-7.3) |
| inner phenyl CH | 109.0 (109.0) | ?[b] (6.6) | 107.8 (109.6) | 6.8 (7.4) |

[a] No such group is present in the molecule. [b] The signal intensity in the 2D REPT-HSQC spectrum is too low to reliably determine the $^1$H chemical shift.

Obviously, the −O− linker provides efficient mechanical decoupling from the phenyl ring, whose dynamics is considerably different in G1-PMA and G2-PMA.

**4.5. G1-4EO-PMA vs G1-PMA.** The G1-4EO-PMA macromolecule is very similar to G1-PMA, with the only difference being a linker of four ethoxy (EO) groups between the polymethacrylate backbone and G1 dendron. G1-4EO-PMA also self-assembles into columns, but the EO linker chain has significant influences. Its impact on the supramolecular structure is quite pronounced, because G1-4EO-PMA displays a higher long-range order than the molecules without EO linker unit, so that detailed small- and wide-angle X-ray diffraction studies could be carried out.[7] By comparing the solid-state NMR data of G1-4EO-PMA and G1-PMA, more insight can be gained into the effects of the linker unit on the local arrangement and dynamics of the phenyl rings. Then the question can be tackled whether these properties can be considered as the actual source of the increased long-range order.

*Chemical Shifts.* In Table 6, selected solid-state chemical shifts of G1-4EO-PMA are compared with the corresponding solution-state values (in brackets) as well as with the values of G1-PMA. Similar to G1-PMA, the $^{13}$C resonances at 68.0 and 74.5 ppm could be assigned to the 4-$OCH_2$R and 4-$OCH_2$Ph groups, respectively. There is only one more resonance observed at 70.3 ppm, which has to be assigned to the 3,5-$OCH_2$Ph groups as well as to the EO linker. Unfortunately, these groups turn out to have the same $^{13}$C chemical shifts. On the basis of the solution-state values in Table 6, different $^1$H chemical-shifts would be expected for 3,5-$OCH_2$Ph and the linker unit in the solid state, but basically only one broad $^1$H resonance at 3.4−3.8 ppm is observed for the different $OCH_2$ groups in the 2D $^1$H−$^{13}$C REPT-HSQC spectrum (shown in Figure 6D). This is in significant contrast to the observation of many different $^1$H chemical shifts in G1-PMA, G1-PS, and G2-PMA (see Figure 6A−C) and leads to the conclusion that the EO linker introduces some degree of flexibility into the system, thereby allowing for a distribution of conformations and, as a consequence of this, a distribution of $^1$H chemical shifts. Correspondingly, a broad Gaussian-type line shape is found, which reflects the distribution of local conformations. It should be noted that the protons of the linker do not experience aromatic ring currents at all but remain at their solution-state resonance position. Hence, the EO linker and the aromatic units are spatially separated in the columns.

*Molecular Dynamics*. Turning to the dynamics of G1-4EO-PMA, the TEDOR spectra in Figure 7D show that the signal of the 4-$OCH_2$R group disappears at four rotor periods excitation while the corresponding signal is still present in the case of G1-PMA (Figure 7A). Hence, the 4-$OCH_2$R group is less mobile in G1-4EO-PMA than in G1-PMA. Moving toward the inner part of the dendron, the 4-$OCH_2$Ph group remains basically as mobile as the 4-$OCH_2$R group. The peak at 70.3 ppm is dominated by the EO linker (concealing the 3,5-$OCH_2$R signal), and its mobility is also comparable to 4-$OCH_2$R. This observation is confirmed by REREDOR spinning sideband patterns (Figure 14), which yield residual heteronuclear couplings of $D_{CH}/2\pi = 11.5$ and 11.0 kHz for the EO linker and the 4-$OCH_2$R group, respectively, corresponding to order parameters $S_{het} = 54-56\%$. Thus, considering all $OCH_2$ segment mobilities, it can be concluded that G1-4EO-PMA exhibits basically no mobility gradient through its dendritic side groups.

For the outer phenyl rings, residual homo- and heteronuclear couplings of $D_{HH}/2\pi = 4.7$ kHz (Figure 10D) and $D_{CH}/2\pi = 6.3$ kHz (Figure 9D), respectively, are found, which are similar

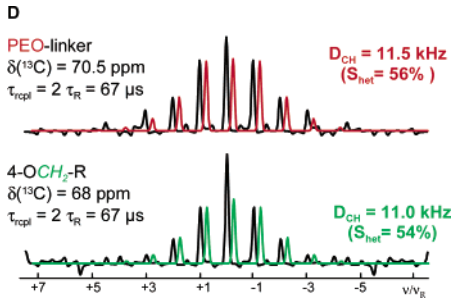


***Figure 14.*** Residual $^1H-^{13}C$ dipolar couplings of the different $OCH_2$ groups of (**D**) G1-4EO-PMA below $T_g$ ($T$ = 15 °C), as measured by REREDOR spinning sideband patterns recorded under MAS at 30 kHz (black line = experimental, colored line = calculated).

to G1-PMA (Figures 10A and 9A). Therefore, the outer phenyl rings of G1-4EO-PMA undergo 180° flips in addition to a motion of the whole side chain with a chain order parameter of $S_{hom} \approx 60\%$, as found for G1-PMA above. This value is not significantly higher than the one determined for the EO linker ($S_{het} = 56\%$) and the 4-$OCH_2$R group ($S_{het} = 54\%$) in G1-4EO-PMA, which again shows that the dendrons of G1-4EO-PMA exhibit a very uniform motion, in contrast to G1-PMA. Obviously, the EO linker mechanically decouples the polymer backbone from the dendron, such that the immobility of the backbone parts no longer induces a mobility gradient through the dendron. In this way, the aromatic units of the dendrons gain motional flexibility, which allows them to unperturbedly arrange in a favorable fashion.

## 5. Conclusion

Dipolar $^1H-^1H$ and $^1H-^{13}C$ recoupling NMR methods under fast MAS allow a detailed analysis of the local structure and the local molecular dynamics in supramolecular dendritic polymers without the need of isotopically enriched materials. The present work focuses on how dendritic side groups attached to a polymer backbone arrange in a supramolecular fashion and how this assembly with its local molecular packing and dynamics is influenced by (i) the polymer backbone, (ii) the generation of dendritic side groups, or (iii) the type and size of linkers. All four polymers investigated self-assemble in a columnar fashion, which is well organized below as well as above $T_g$.

High local dynamical order parameters of up to $S = 100\%$, as obtained from $^1H-^{13}C$ and $^1H-^1H$ dipolar recoupling experiments, and pronounced aromatic ring-current effects on $^1H$ chemical shifts, as observed in $^1H-^{13}C$ correlation spectra, provide evidence for a high degree of order in the packing of the dendrons. The pronounced local order among the aromatic moieties implies that these parts play a structure-directing role in the systems. Using aromatic ring current effects on $^1H$ chemical shifts as distance constraints, "edge-on"- and "face-on"-type arrangements can be identified as characteristic features of the dendron packing. Within the dendrons (except for G1-4EO-PMA, see below), large mobility gradients are found to range from $S_{het} \approx 100\%$ for the inner phenyl rings to $S_{het} \approx 30\%$ for the outer ones. Hence, the core of the column consists of a helical polymer backbone which is surrounded by the inner, well-organized, and relatively rigid part of the dendrons. At the outer part of the dendrons, mobile dodecyl chains build an additional flexible layer toward the surface of the columns, which further stabilizes them.

Besides these common general features, a more detailed study of the individual properties of the dendritic polymers reveals further similarities as well as a few significant differences among them. G1-PMA and G1-PS generally exhibit very similar overall properties: They do not differ much in their $T_g$ value and their melting temperature, and a very similar arrangement of the dendritic moieties of G1-PMA and G1-PS is observed. The $\pi$-shifts experienced by the $OCH_2$Ph protons are largely identical for both systems, which indicates similar ring-current effects and, thus, implies that the arrangement of the aromatic rings and $OCH_2$ groups must be essentially the same for G1-PMA and G1-PS. This is further confirmed by the similar dynamical properties observed for both systems. From this comparison, it is obvious that the polymer backbone does not have a significant influence on the structure adopted by the system. Rather, the aromatic moieties in the dendrons are the driving force in the self-assembly process, inducing a helical arrangement of both the PS and the PMA chain.

Comparing dendrons of first and second generation (i.e., G1-PMA vs G2-PMA), the $OCH_2$ groups and aromatic rings of the G2-dendron arrange in a fashion comparable to G1. In G2, however, more pronounced $\pi$-shifts are observed, which indicate a higher density of phenyl rings around the $OCH_2$ groups. In general, less motion is observed in the G2-dendrons than in G1, which can predominantly be attributed to steric effects associated with the 3,4,5-substitution of O-dodecyl chains in G2.

G1-4EO-PMA deviate significantly from the other three materials. Here, the flexible EO linker unit provides efficient mechanical decoupling between the polymer backbone and the attached dendron, such that the latter can arrange in a favorable fashion ($S_{het}$ = 54%-56%) instead of being forced to mediate between the rigid backbone and the flexible alkyl chains. The different arrangement of the G1-dendrons in G1-PMA and G1-4EO-PMA is also reflected by the very different ring current effects on the $^1H$ chemical shifts detected for the two systems. Remarkably, G1-4EO-PMA exhibits a higher long-range order below $T_g$.

In conclusion, this investigation shows how advanced solid-state NMR experiments can elucidate the local structure of supramolecular architectures as well as the site-specific dynamics of different molecular building blocks in large complex systems. In this way, valuable information is provided which helps to quantify local interactions, to identify structure-directing elements, and to understand order phenomena, which all together determine the self-assembly process of supramolecular systems.

**Acknowledgment.** The authors thank the Deutsche Forschungsgemeinschaft (DFG, SFB 625 in Mainz) and the National Science Foundation, USA for financial support.

JA035127D